Exotic disordered phases in the quantum J_1-J_2 model on the honeycomb lattice

Hao Zhang[1,*] and C. A. Lamas[2]

[1]*Institute for Solid State Physics, University of Tokyo, Kashiwa, Chiba 277-8581, Japan*

[2]*Laboratoire de Physique Théorique, IRSAMC, CNRS and Université de Toulouse, UPS, F-31062 Toulouse, France*

(Received 26 September 2012; revised manuscript received 12 December 2012; published 22 January 2013)

We study the ground-state phase diagram of the frustrated quantum J_1-J_2 Heisenberg antiferromagnet on the honeycomb lattice using a mean-field approach in terms of the Schwinger boson representation of the spin operators. We present results for the ground-state energy, local magnetization, energy gap, and spin-spin correlations. The system shows magnetic long-range order for $0 \leqslant J_2/J_1 \lesssim 0.2075$ (Néel) and $0.398 \lesssim J_2/J_1 \leqslant 0.5$ (spiral). In the intermediate region, we find two magnetically disordered phases: a gapped spin liquid phase, which shows short-range Néel correlations ($0.2075 \lesssim J_2/J_1 \lesssim 0.3732$), and a lattice nematic phase ($0.3732 \lesssim J_2/J_1 \lesssim 0.398$), which is magnetically disordered but breaks lattice rotational symmetry. The errors in the values of the phase boundaries, which are implicit in the number of significant figures quoted, correspond purely to the error in the extrapolation of our finite-size results to the thermodynamic limit.

DOI: 10.1103/PhysRevB.87.024415 PACS number(s): 75.10.Kt, 75.10.Jm, 75.50.Ee

I. INTRODUCTION

The two-dimensional (2D) Heisenberg model on bipartite lattices has been intensively studied in recent years. In the unfrustrated case, the classical ground state is obtained when all the spins in one sublattice are pointing in a given direction while in the other sublattice the spins are pointing in the opposite direction. However, in the quantum case this state is not the real ground state; in fact this is not an eigenstate of the Hamiltonian. The quantum ground state is exactly known in one dimension,[1] but no exact results for the two-dimensional antiferromagnet are known, even for simple lattices like the square lattice. However, several experimental and numerical studies suggested that the ground state is in fact the spin SU(2) symmetry-broken Néel-type state. In contrast, when we include frustration in the system, for example, by including second-nearest-neighbor interactions, the ground state may become much more complicated.

In the quantum case, the ground-state energy is lower than the classical value due to the quantum fluctuations. The effects of these fluctuations vary depending on the dimension, the spin quantum number, the presence of frustrating interactions, and the coordination number of the lattice. One can ask what the quantum fluctuations are when the coordination number is changed. In two dimensions two paradigmatic examples of unfrustrated systems are the square lattice, with coordination number $z = 4$, and the honeycomb lattice, with $z = 3$. Previous results[2,3] have shown that the staggered magnetization is smaller in the $z = 3$ case. This behavior is in accord with the tendency towards a less classical behavior for systems with a lower coordination number.

The inclusion of frustration in 2D quantum antiferromagnets is expected to enhance the effect of quantum spin fluctuations and hence suppress magnetic order.[4] This idea has motivated many researchers to look for its realization.[5–9] A special scenario to check this is the frustrated Heisenberg model on the honeycomb lattice. Due to the small coordination number ($z = 3$), which is the lowest allowed in a 2D system, quantum fluctuations could be expected to be stronger than those on the square lattice and may destroy the antiferromagnetic order.[10–13]

The study of frustrated quantum magnets on the honeycomb lattice has also experimental motivations.[14–20] One of the most exciting experimental progresses is one kind of bismuth oxynitrate, $Bi_3Mn_4O_{12}(NO_3)$, which was obtained by Smirnova *et al.*[14] In this compound the Mn^{4+} ions form a $S = 3/2$ honeycomb lattice without any distortion. The magnetic susceptibility data indicate two-dimensional magnetism. Despite the large antiferromagnetic Weiss constant of −257 K, no long-range ordering was observed down to 0.4 K, which suggests a nonmagnetic ground state.[14–17] The substitution of Mn^{4+} in $Bi_3Mn_4O_{12}(NO_3)$ by V^{4+} may lead to the realization of the $S = 1/2$ Heisenberg model on the honeycomb lattice.

The analysis of the honeycomb lattice from a more general point of view has gained lately a lot of interest both from graphene-related issues[21] and from the possible spin-liquid phase found in the Hubbard model in such geometry.[22–29] Due to these reasons, recently there has been huge theoretical interest in frustrated Heisenberg models on the honeycomb lattice, in which frustration is incorporated by second-nearest-neighbor couplings[23,30–37] and maybe also third-nearest-neighbor couplings.[38–45]

Motivated by previous results, in this paper we study the spin-1/2 Heisenberg model on the honeycomb lattice with first (J_1) and second (J_2) nearest-neighbor couplings. Using a Schwinger boson mean-field theory (SBMFT), we find strong evidence for the existence of an intermediate disordered region where a spin gap opens and spin-spin correlations decay exponentially. This magnetically disordered region quantitatively agrees well with recent numerical simulation results.[36,37,39,45] Another key finding of our work is the presence of two kinds of magnetically disordered phases in this region. One is a gapped spin liquid (GSL)[46,47] with short-range Néel correlations, maintaining the lattice translational and rotational symmetry. The other phase is a staggered-dimer valence-bond crystal (VBC), which is also called lattice nematic.[30] This phase breaks lattice rotational symmetry but preserves lattice translational symmetry.

The rest of this paper is arranged as follows. In Sec. II we introduce our model and give a quick overview of the final phase diagram. In Sec. III the general formalism of the

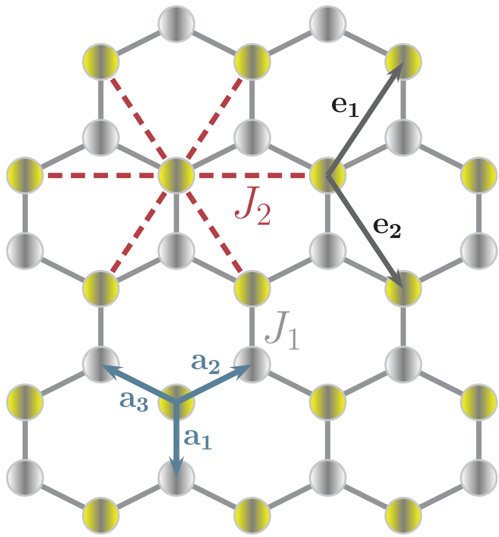

FIG. 1. (Color online) The honeycomb lattice with the J_1 and J_2 couplings considered in this paper. The lattice sites with different colors belong to different sublattices. The primitive translation vectors of the direct lattice are $\mathbf{e}_1 = (\sqrt{3}/2, 3/2)$ and $\mathbf{e}_2 = (\sqrt{3}/2, -3/2)$. $\mathbf{a}_1 = (0, -1)$, $\mathbf{a}_2 = (\sqrt{3}/2, 1/2)$, and $\mathbf{a}_3 = (-\sqrt{3}/2, 1/2)$ correspond to the nearest neighbor bonds.

Schwinger boson mean-field approach is presented. In Sec. IV, using the solutions of mean-field equations, we discuss the phase diagram, especially the magnetically disordered region. We close with a summary and discussion in Sec. V.

II. MODEL AND OVERVIEW OF THE PHASE DIAGRAM

The J_1-J_2 Heisenberg model on the honeycomb lattice is given by

$$H = J_1 \sum_{\langle \mathbf{xy} \rangle_1} \hat{\mathbf{S}}_\mathbf{x} \cdot \hat{\mathbf{S}}_\mathbf{y} + J_2 \sum_{\langle \mathbf{xy} \rangle_2} \hat{\mathbf{S}}_\mathbf{x} \cdot \hat{\mathbf{S}}_\mathbf{y}, \tag{1}$$

where $\hat{\mathbf{S}}_\mathbf{x}$ is the spin operator on site $\mathbf{x}$ and $\langle \mathbf{xy} \rangle_n$ indicates the sum over the nth neighbors (see Fig. 1). In this paper we are interested in the antiferromagnetic case ($J_1, J_2 \geqslant 0$), and we focus on the region $J_2/J_1 \in [0, 0.5]$.

In the classical limit, $S \to \infty$, the model displays different zero-temperature phases;[48–50] see Fig. 2(a). For $J_2/J_1 < 1/6$, the system is Néel ordered, while for $J_2/J_1 > 1/6$, the system shows spiral phases. For the quantum case, aspects of this model have been explored previously in the literature by various approaches, including spin wave theory,[30,31,49,50] a nonlinear σ-model approach,[51] mean-field theory,[10,23] exact diagonalization (ED),[34,39,50] a variational Monte Carlo (VMC) method,[33,36] series expansion (SE),[40] the pseudofermion functional renormalization group (PFFRG),[42] and the coupled-cluster method (CCM).[37] However, these works yielded conflicting physical scenarios.

This model was studied by Mattsson *et al.*[10] using SBMFT with a mean-field decoupling that considers only antiferromagnetic correlations for nearest neighbors and ferromagnetic correlations for next-nearest neighbors. This scheme can only correctly describe Néel order. More recently, Wang[23] studied this model within SBMFT including antiferromagnetic correlations for both nearest and next-nearest neighbors.

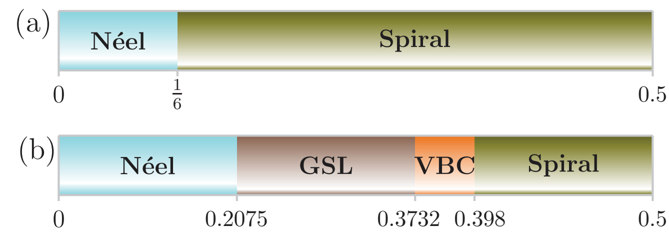

FIG. 2. (Color online) Phase diagram as a function of the frustration J_2/J_1. (a) Classical phase diagram. (b) Quantum phase diagram corresponding to $S = \frac{1}{2}$ obtained by means of SBMFT.

Unfortunately, the author did not give the phase diagram for different values of J_2/J_1. Actually, for frustrated models we cannot generally exclude either ferromagnetic or antiferromagnetic correlations,[52] and it is important to use a mean-field decomposition that allows us to include ferromagnetic and antiferromagnetic correlations on equal footing. Another point is that both of them assume the bond mean fields are independent of the directions of the bonds. Therefore, these two schemes cannot describe the phases in which the lattice rotational symmetry has broken. Here we study Hamiltonian (1) in the strong quantum limit ($S = 1/2$) using a rotationally invariant version of this technique, which has proven successful in incorporating quantum fluctuations.[38,52–58]

Our main results are summarized in Fig. 2(b). The magnetic phase diagram is divided into four regions.[59] At small values of the frustrating coupling J_2/J_1, the system presents a Néel-like ground state. By increasing the frustration, we find at $J_2/J_1 \simeq 0.2075$ a continuous transition to a gapped spin liquid phase. When the value of the frustrating coupling exceeds $J_2/J_1 \simeq 0.3732$, we find a continuous transition into a staggered-dimer VBC (lattice nematic) with broken Z_3 symmetry (see Fig. 3), which transforms at $J_2/J_1 \simeq 0.398$ into a spiral phase.

III. SCHWINGER BOSON MEAN-FIELD APPROACH

It is well known that the SBMFT provides a natural description for both magnetically ordered and disordered phases based on the picture of the resonating valence bond states.[4,60–62] As a plus, this method does not start from any

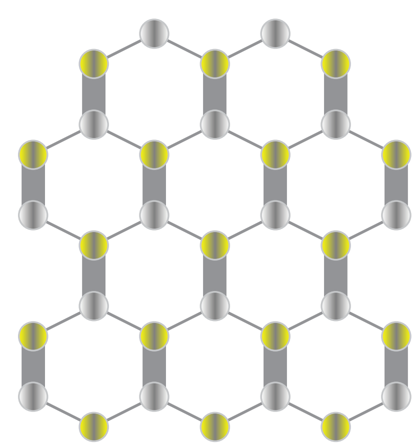

FIG. 3. (Color online) Sketch of the staggered-dimer VBC state which breaks the lattice rotational symmetry but preserves the lattice translational symmetry.

magnetic long-range order for the ground state (in contrast to spin-wave theory), which should emerge naturally if the Schwinger bosons condense at some momentum vector.[63] At this momentum vector, the lowest excitation spectrum of the Schwinger bosons should be gapless. On the other hand, if the Schwinger bosons are gapped, the phase is magnetically disordered. In the following, we will present in detail the rotationally invariant version of SBMFT which was introduced by Ceccatto *et al.*[53–55] and which we use in the following sections.

Consider the SU(2) Heisenberg Hamiltonian on a general lattice:

$$\hat{H} = \frac{1}{2}\sum_{\mathbf{xy}\alpha\beta} J_{\alpha\beta}(\mathbf{x}-\mathbf{y})\hat{\mathbf{S}}_{\mathbf{x}+\mathbf{r}_\alpha}\cdot\hat{\mathbf{S}}_{\mathbf{y}+\mathbf{r}_\beta}, \tag{2}$$

where $\mathbf{x}$ and $\mathbf{y}$ are the positions of the unit cells and vectors $\mathbf{r}_\alpha$ are the positions of each atom within the unit cell. $J_{\alpha\beta}(\mathbf{x}-\mathbf{y})$ is the exchange interaction between the spins located in $\mathbf{x}+\mathbf{r}_\alpha$ and $\mathbf{y}+\mathbf{r}_\beta$.

In what follows we assume that the classical order can be parameterized as

$$\hat{S}^x_{\mathbf{x}+\mathbf{r}_\alpha} = S\sin\varphi_\alpha(\mathbf{x}), \tag{3}$$

$$\hat{S}^y_{\mathbf{x}+\mathbf{r}_\alpha} = 0, \tag{4}$$

$$\hat{S}^z_{\mathbf{x}+\mathbf{r}_\alpha} = S\cos\varphi_\alpha(\mathbf{x}), \tag{5}$$

with $\varphi_\alpha(\mathbf{x}) = \mathbf{Q}\cdot\mathbf{x}+\theta_\alpha$, where $\mathbf{Q}$ is the ordering vector and θ_α are the relative angles between the classical spins inside each unit cell.

The spin operators $\hat{\mathbf{S}}_\mathbf{x}$ on site $\mathbf{x}$ are represented by two bosons $\hat{b}_{\mathbf{x}\sigma}$ $(\sigma=\uparrow,\downarrow)$,

$$\hat{\mathbf{S}}_\mathbf{r} = \frac{1}{2}\,\hat{\mathbf{b}}^\dagger_\mathbf{r}\cdot\vec{\sigma}\cdot\hat{\mathbf{b}}_\mathbf{r}, \quad \hat{\mathbf{b}}_\mathbf{r} = \begin{pmatrix}\hat{b}_{\mathbf{r}\uparrow}\\ \hat{b}_{\mathbf{r}\downarrow}\end{pmatrix}, \tag{6}$$

where $\vec{\sigma} = (\sigma_x,\sigma_y,\sigma_z)$ are the Pauli matrices. Equation (6) is a faithful representation of the algebra SU(2) if we take into account the following local constraint:

$$2S = \hat{b}^\dagger_{\mathbf{x}\uparrow}\hat{b}_{\mathbf{x}\uparrow} + \hat{b}^\dagger_{\mathbf{x}\downarrow}\hat{b}_{\mathbf{x}\downarrow}. \tag{7}$$

The exchange term can be expressed as

$$\hat{\mathbf{S}}_{\mathbf{x}+\mathbf{r}_\alpha}\cdot\hat{\mathbf{S}}_{\mathbf{y}+\mathbf{r}_\beta} = :\hat{B}^\dagger_{\alpha\beta}(\mathbf{x},\mathbf{y})\hat{B}_{\alpha\beta}(\mathbf{x},\mathbf{y}): -\hat{A}^\dagger_{\alpha\beta}(\mathbf{x},\mathbf{y})\hat{A}_{\alpha\beta}(\mathbf{x},\mathbf{y}), \tag{8}$$

where $\hat{A}_{\alpha,\beta}(\mathbf{x},\mathbf{y})$ and $\hat{B}_{\alpha,\beta}(\mathbf{x},\mathbf{y})$ are SU(2) invariants defined as

$$\hat{A}_{\alpha,\beta}(\mathbf{x},\mathbf{y}) = \frac{1}{2}\sum_\sigma \sigma\hat{b}^{(\alpha)}_{\mathbf{x},\sigma}\hat{b}^{(\beta)}_{\mathbf{y},-\sigma}, \tag{9}$$

$$\hat{B}_{\alpha,\beta}(\mathbf{x},\mathbf{y}) = \frac{1}{2}\sum_\sigma \hat{b}^{\dagger(\alpha)}_{\mathbf{x},\sigma}\hat{b}^{(\beta)}_{\mathbf{y},\sigma}, \tag{10}$$

with $\sigma=\uparrow,\downarrow$. The double dots $(:\hat{O}:)$ indicate the normal ordering of operator $\hat{O}$. This decoupling is particularly useful in the study of magnetic systems near disordered phases because it allows us to treat antiferromagnetism and ferromagnetism on equal footing.[52–55] On the other hand, this scheme has been tested to obtain quantitatively quite accurate results which show excellent agreements with ED.[38,53–55]

To construct a mean-field Hamiltonian we perform the following Hartree-Fock decoupling:

$$\begin{aligned}(\hat{\mathbf{S}}_{\mathbf{x}+\mathbf{r}_\alpha}\cdot\hat{\mathbf{S}}_{\mathbf{y}+\mathbf{r}_\beta})_{MF} &= [B^*_{\alpha\beta}(\mathbf{x}-\mathbf{y})\hat{B}_{\alpha\beta}(\mathbf{x},\mathbf{y}) - A^*_{\alpha\beta}(\mathbf{x}-\mathbf{y})\hat{A}_{\alpha\beta}(\mathbf{x},\mathbf{y}) + \text{H.c.}]\\ &\quad -\langle(\hat{\mathbf{S}}_{\mathbf{x}+\mathbf{r}_\alpha}\cdot\hat{\mathbf{S}}_{\mathbf{y}+\mathbf{r}_\beta})_{MF}\rangle,\end{aligned} \tag{11}$$

where we have defined

$$A^*_{\alpha\beta}(\mathbf{x}-\mathbf{y}) = \langle\hat{A}^\dagger_{\alpha\beta}(\mathbf{x},\mathbf{y})\rangle, \tag{12}$$

$$B^*_{\alpha\beta}(\mathbf{x}-\mathbf{y}) = \langle\hat{B}^\dagger_{\alpha\beta}(\mathbf{x},\mathbf{y})\rangle, \tag{13}$$

$$\langle(\hat{\mathbf{S}}_{\vec{x}+\vec{r}_\alpha}\cdot\hat{\mathbf{S}}_{\vec{y}+\vec{r}_\beta})_{MF}\rangle = |B_{\alpha\beta}(\vec{x}-\vec{y})|^2 - |A_{\alpha\beta}(\vec{x}-\vec{y})|^2$$

and $\langle\,\rangle$ denotes the expectation value in the ground state at $T=0$. It is convenient to change variables to $\mathbf{R}=\mathbf{x}-\mathbf{y}$, and eliminating $\mathbf{x}$ in the sums, we obtain

$$\begin{aligned}\hat{H}_{MF} = \frac{1}{2}\sum_{\mathbf{R}\mathbf{y}\alpha\beta} J_{\alpha\beta}(\mathbf{R})\Bigg\{&\frac{1}{2}\sum_\sigma\big[B_{\alpha,\beta}(\mathbf{R})\,\hat{b}^{\dagger(\alpha)}_{\mathbf{R}+\mathbf{y},\sigma}\hat{b}^{(\beta)}_{\mathbf{y},\sigma}\\ &-\sigma A_{\alpha,\beta}(\mathbf{R})\,\hat{b}^{\dagger(\alpha)}_{\mathbf{R}+\mathbf{y},\sigma}\hat{b}^{\dagger(\beta)}_{\mathbf{y},-\sigma} + \text{H.c.}\big]\\ &-[|B_{\alpha,\beta}(\mathbf{R})|^2 - |A_{\alpha,\beta}(\mathbf{R})|^2]\Bigg\}.\end{aligned}$$

The mean-field Hamiltonian is quadratic in the boson operators and can be diagonalized. It is convenient to transform the operators to momentum space

$$\hat{b}^{(\alpha)}_{\mathbf{x},\sigma} = \frac{1}{\sqrt{N_c}}\sum_\mathbf{k}\hat{b}^{(\alpha)}_{\mathbf{k},\sigma}e^{i\mathbf{k}\cdot(\mathbf{x}+\mathbf{r}_\alpha)}, \tag{14}$$

where N_c is the number of unit cells. After some algebra and using the symmetry properties

$$\begin{aligned}J_{\alpha\beta}(\mathbf{R}) &= J_{\beta\alpha}(-\mathbf{R}),\\ A_{\alpha\beta}(\mathbf{R}) &= -A_{\beta\alpha}(-\mathbf{R}),\\ B_{\alpha\beta}(\mathbf{R}) &= B^*_{\beta\alpha}(-\mathbf{R}),\end{aligned} \tag{15}$$

we obtain the following form for the Hamiltonian:

$$\begin{aligned}\hat{H}_{MF} = \frac{1}{2}\sum_{\mathbf{k}\alpha\beta}\sum_\sigma\{&\gamma^B_{\alpha\beta}(\mathbf{k})\hat{b}^{\dagger(\alpha)}_{\mathbf{k}\sigma}\hat{b}^{(\beta)}_{\mathbf{k}\sigma} + \gamma^B_{\alpha\beta}(-\mathbf{k})\hat{b}^{\dagger(\alpha)}_{-\mathbf{k}-\sigma}\hat{b}^{(\beta)}_{-\mathbf{k}-\sigma}\\ &-\sigma\gamma^A_{\alpha\beta}(\mathbf{k})\hat{b}^{\dagger(\alpha)}_{\mathbf{k}\sigma}\hat{b}^{\dagger(\beta)}_{-\mathbf{k}-\sigma} - \sigma\bar{\gamma}^A_{\alpha\beta}(\mathbf{k})\hat{b}^{(\alpha)}_{\mathbf{k}\sigma}\hat{b}^{(\beta)}_{-\mathbf{k}-\sigma}\}\\ &-\frac{N_c}{2}\sum_{\mathbf{R}\alpha\beta}J_{\alpha\beta}(\mathbf{R})[|B_{\alpha\beta}(\mathbf{R})|^2 - |A_{\alpha\beta}(\mathbf{R})|^2],\end{aligned} \tag{16}$$

where

$$\gamma^B_{\alpha\beta}(\mathbf{k}) = \frac{1}{2}\sum_\mathbf{R}J_{\alpha\beta}(\mathbf{R})B_{\alpha\beta}(\mathbf{R})e^{-i\mathbf{k}\cdot(\mathbf{R}+\mathbf{r}_\alpha-\mathbf{r}_\beta)}, \tag{17}$$

$$\gamma^A_{\alpha\beta}(\mathbf{k}) = \frac{1}{2}\sum_\mathbf{R}J_{\alpha\beta}(\mathbf{R})A_{\alpha\beta}(\mathbf{R})e^{-i\mathbf{k}\cdot(\mathbf{R}+\mathbf{r}_\alpha-\mathbf{r}_\beta)}, \tag{18}$$

$$\bar{\gamma}^A_{\alpha\beta}(\mathbf{k}) = \frac{1}{2}\sum_\mathbf{R}J_{\alpha\beta}(\mathbf{R})\bar{A}_{\alpha\beta}(\mathbf{R})e^{-i\mathbf{k}\cdot(\mathbf{R}+\mathbf{r}_\alpha-\mathbf{r}_\beta)}. \tag{19}$$

Now, we impose constraint (7) on average over each sublattice α by means of Lagrange multipliers $\lambda^{(\alpha)}$,

$$\hat{H}_{MF} \to \hat{H}_{MF} + \hat{H}_\lambda, \tag{20}$$

with

$$\hat{H}_\lambda = \sum_{\mathbf{x}\alpha} \lambda^{(\alpha)} \left(\sum_\sigma \hat{b}^{\dagger(\alpha)}_{\mathbf{x}\sigma} \hat{b}^{(\alpha)}_{\mathbf{x}\sigma} - 2S \right). \tag{21}$$

Using symmetries (15), we can see that both kinds of bosons $(\uparrow,\downarrow)$ give the same contribution to the Hamiltonian. Then, we can perform the sum over σ to obtain

$$\begin{aligned}\hat{H}_{MF} = &\frac{1}{2}\sum_{\mathbf{k}\alpha\beta} \{(\gamma^B_{\alpha\beta}(\mathbf{k}) + \lambda^{(\alpha)}\delta_{\alpha\beta})\hat{b}^{\dagger(\alpha)}_{\mathbf{k}\uparrow}\hat{b}^{(\beta)}_{\mathbf{k}\uparrow} + [\gamma^B_{\alpha\beta}(-\mathbf{k})\\ &+ \lambda^{(\alpha)}\delta_{\alpha\beta}]\hat{b}^{\dagger(\alpha)}_{-\mathbf{k}\downarrow}\hat{b}^{(\beta)}_{-\mathbf{k}\downarrow} - \sigma[\gamma^A_{\alpha\beta}(\mathbf{k})\hat{b}^{\dagger(\alpha)}_{\mathbf{k}\uparrow}\hat{b}^{\dagger(\beta)}_{-\mathbf{k}\downarrow}\\ &+ \bar{\gamma}^A_{\alpha\beta}(\mathbf{k})\hat{b}^{(\alpha)}_{\mathbf{k}\uparrow}\hat{b}^{(\beta)}_{-\mathbf{k}\downarrow}]\} - \frac{N_c}{2}\sum_{\mathbf{R}\alpha\beta} J_{\alpha\beta}(\mathbf{R})[|B_{\alpha\beta}(\mathbf{R})|^2\\ &- |A_{\alpha\beta}(\mathbf{R})|^2] - 2SN_c\sum_\alpha \lambda^{(\alpha)}.\end{aligned}$$

It is convenient to introduce the Nambu spinor $\hat{\mathbf{b}}^\dagger(\mathbf{k}) = (\hat{\mathbf{b}}^\dagger_{\mathbf{k}\uparrow}, \hat{\mathbf{b}}_{-\mathbf{k}\downarrow})$, where

$$\hat{\mathbf{b}}^\dagger_{\mathbf{k}\uparrow} = (\hat{b}^{\dagger(\alpha_1)}_{\mathbf{k}\uparrow}, \hat{b}^{\dagger(\alpha_2)}_{\mathbf{k}\uparrow}, \ldots, \hat{b}^{\dagger(\alpha_{n_c})}_{\mathbf{k}\uparrow}), \tag{22}$$

$$\hat{\mathbf{b}}_{-\mathbf{k}\downarrow} = (\hat{b}^{\dagger(\alpha_1)}_{-\mathbf{k}\downarrow}, \hat{b}^{\dagger(\alpha_2)}_{-\mathbf{k}\downarrow}, \ldots, \hat{b}^{\dagger(\alpha_{n_c})}_{-\mathbf{k}\downarrow}), \tag{23}$$

and n_c is the number of atoms in the unit cell. Now, we can rewrite the Hamiltonian into a compact form:

$$\begin{aligned}H_{MF} = &\sum_{\mathbf{k}} \hat{\mathbf{b}}^\dagger(\mathbf{k}) \cdot D(\mathbf{k}) \cdot \hat{\mathbf{b}}(\mathbf{k})\\ &- (2S+1)N_c \sum_\alpha \lambda^{(\alpha)} - \langle H_{MF}\rangle,\end{aligned} \tag{24}$$

where the $2\,n_c \times 2\,n_c$ dynamical matrix $D(\mathbf{k})$ is given by

$$D(\mathbf{k}) = \begin{pmatrix} \gamma^B_{\alpha\beta}(\mathbf{k}) + \lambda^{(\alpha)}\delta_{\alpha\beta} & -\gamma^A_{\alpha\beta}(\mathbf{k}) \\ \gamma^A_{\alpha\beta}(\mathbf{k}) & \gamma^B_{\alpha\beta}(\mathbf{k}) + \lambda^{(\alpha)}\delta_{\alpha\beta} \end{pmatrix}.$$

To diagonalize the Hamiltonian (24) we need to perform a paraunitary transformation of the matrix $D(\mathbf{k})$ which preserves the bosonic commutation relations.[64] We can diagonalize the Hamiltonian by defining the new operators $\hat{\mathbf{a}} = F \cdot \hat{\mathbf{b}}$, where the matrix F satisfies

$$(F^\dagger)^{-1} \cdot \tau_3 \cdot (F)^{-1} = \tau_3, \quad \tau_3 = \begin{pmatrix} I_{2\times 2} & 0 \\ 0 & -I_{2\times 2} \end{pmatrix}. \tag{25}$$

With this transformation, the Hamiltonian reads

$$\hat{H}_{MF} = \sum_{\mathbf{k}} \hat{\mathbf{a}}^\dagger_{\mathbf{k}} \cdot \mathbf{E}(\mathbf{k}) \cdot \hat{\mathbf{a}}_{\mathbf{k}} - (2S+1)N_c \sum_\alpha \lambda^{(\alpha)} - \langle \hat{H}_{MF}\rangle, \tag{26}$$

where

$$\mathbf{E}(\mathbf{k}) = \mathrm{diag}[\omega_1(\mathbf{k}), \ldots, \omega_{n_c}(\mathbf{k}), \omega_1(\mathbf{k}), \ldots, \omega_{n_c}(\mathbf{k})]. \tag{27}$$

In terms of the original bosonic operators, the mean-field parameters are

$$\begin{aligned}A_{\alpha\beta}(\mathbf{R}) = &\frac{1}{2N_c}\sum_{\mathbf{k}} \{e^{i\mathbf{k}(\mathbf{R}+\mathbf{r}_\alpha-\mathbf{r}_\beta)}\langle \hat{b}^{(\alpha)}_{\mathbf{k}\uparrow}\hat{b}^{(\beta)}_{-\mathbf{k}\downarrow}\rangle\\ &- e^{-i\mathbf{k}(\mathbf{R}+\mathbf{r}_\alpha-\mathbf{r}_\beta)}\langle \hat{b}^{(\alpha)}_{-\mathbf{k}\downarrow}\hat{b}^{(\beta)}_{\mathbf{k}\uparrow}\rangle\},\end{aligned} \tag{28}$$

$$\begin{aligned}B_{\alpha\beta}(\mathbf{R}) = &\frac{1}{2N_c}\sum_{\mathbf{k}} \{e^{i\mathbf{k}(\mathbf{R}+\mathbf{r}_\alpha-\mathbf{r}_\beta)}\langle \hat{b}^{\dagger(\beta)}_{\mathbf{k}\uparrow}\hat{b}^{(\alpha)}_{\mathbf{k}\uparrow}\rangle\\ &- e^{-i\mathbf{k}(\mathbf{R}+\mathbf{r}_\alpha-\mathbf{r}_\beta)}\langle \hat{b}^{\dagger(\beta)}_{-\mathbf{k}\downarrow}\hat{b}^{(\alpha)}_{-\mathbf{k}\downarrow}\rangle\},\end{aligned} \tag{29}$$

and the constraint in the number of bosons can be written in the momentum space as

$$\sum_{\mathbf{k}} \{\langle \hat{b}^{\dagger(\alpha)}_{\mathbf{k}\uparrow}\hat{b}^{(\alpha)}_{\mathbf{k}\uparrow}\rangle + \langle \hat{b}^{\dagger(\alpha)}_{-\mathbf{k}\downarrow}\hat{b}^{(\alpha)}_{-\mathbf{k}\downarrow}\rangle\} = 2SN_c, \tag{30}$$

where N_c is the total number of unit cells and S is the spin strength. The mean-field equations (28) and (29) must be solved in a self-consistent way together with the constraints (30) on the number of bosons.

Finding numerical solutions involves finding the roots of the coupled nonlinear equations for the parameters A and B, plus the additional constraints to determine the values of the Lagrange multipliers $\lambda^{(\alpha)}$. We perform the calculations for finite but very large lattices, and finally, we extrapolate the results to the thermodynamic limit.

We solve numerically for different values of the frustration parameter J_2/J_1 and with the values obtained for the MF parameters and the Lagrange multipliers we compute the energy and the new values for the MF parameters. We repeat this self-consistent procedure until the energy and the MF parameters converge. After reaching convergence, we can compute all physical quantities, such as the energy, the excitation gap, the spin-spin correlation, and the local magnetization. During the calculation, it is convenient to fix the energy scale by setting the value of the nearest-neighbor coupling $J_1 = 1$.

IV. RESULTS

In Fig. 4, we show the boson dispersion relation gap extrapolated to the thermodynamic limit as a function of the frustration (J_2/J_1). In the gapped region, the absence of Bose condensation indicates that the ground state is magnetically disordered. This result agrees well with recent ED,[39] VMC,[36] and CCM[37,45] studies. In the gapless region, the excitation spectrum is zero at a given wave vector $\mathbf{k}^* = \mathbf{Q}/2$, where the Boson condensation occurs. This is characteristic of the magnetically ordered phases. The structure of these phases can be understood through the spin-spin correlation function (SSCF) and the excitation spectrum. Some typical examples for different phases will be shown later.

To pin down the precise phase boundaries between the magnetically ordered and disordered phases, we introduce the local magnetization $M(\mathbf{Q})$ as an order parameter, which is obtained from the long-distance SSCF:[53,54]

$$\lim_{|\mathbf{x}-\mathbf{y}|\to\infty} \langle \mathbf{S}_{\mathbf{x}} \cdot \mathbf{S}_{\mathbf{y}}\rangle \approx M^2(\mathbf{Q}) \cos[\mathbf{Q}\cdot(\mathbf{x}-\mathbf{y})]. \tag{31}$$

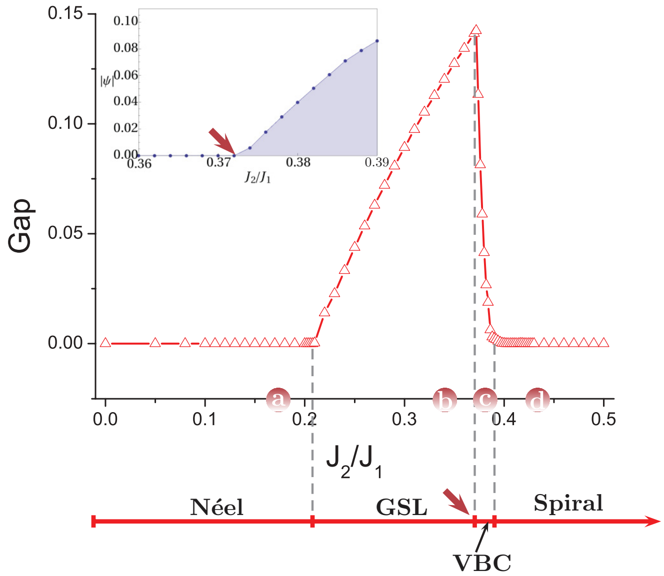

FIG. 4. (Color online) Gap in the boson dispersion extrapolated to the thermodynamic limit as a function of the frustration J_2/J_1 corresponding to $S = 1/2$. The gapped region corresponds to two different magnetically disordered phases: one is GSL, and the other is a staggered-dimer VBC. The inset shows the Z_3 order parameter defined in Eq. (32). The onset of the VBC phase is determined by the value of J_2/J_1 where $|\psi|$ is nonzero (red arrows).

In Fig. 5, we show the local magnetization for $J_2/J_1 \in [0,0.5]$. For $J_2/J_1 = 0$, the local magnetization is $M(\mathbf{Q})$ =0.24176, which is in excellent agreement with the second-order spin-wave calculation result of 0.2418.[65] This value is significantly reduced by quantum fluctuations compared with the classical value of 0.5. The quantum Monte Carlo (QMC) result[66] is 0.2677(6), which is considerably larger than ours. For the unfrustrated case, all the mean-field approaches are quite inaccurate compared with much more controlled techniques like QMC. The difference in the $M(\mathbf{Q})$ values of about 10%

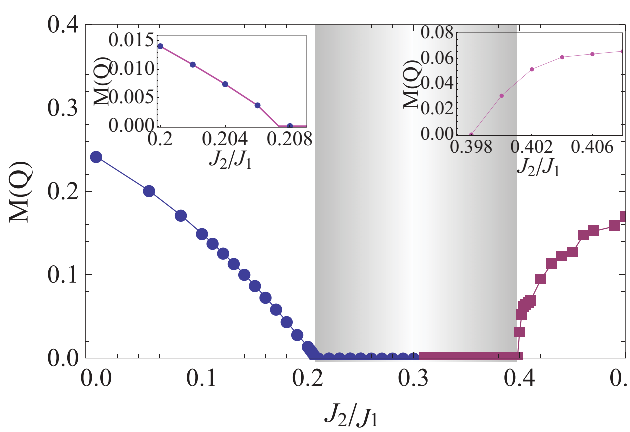

FIG. 5. (Color online) Local magnetization determined by Eq. (31) extrapolated to the thermodynamic limit as a function of the frustration J_2/J_1. The shaded region corresponds to the magnetically disordered phases. Insets correspond to the regions where the magnetization for Néel (left) and spiral (right) phases becomes zero.

provides, in the absence of any other quantitative evidence for the accuracy of the method as applied to this model, an indication of the accuracy of the method and of all the results quoted that depend on the order parameters, including the phase boundaries. However, the mean-field approach is still very useful to study gapped phases in frustrated systems. On one hand, it is well known that for frustrated systems QMC presents the famous sign problem. On the other hand, the study of quantities like energy gap requires the study of large-size clusters, and the use of exact diagonalization for small-size clusters makes it very difficult to extrapolate the results.

As J_2/J_1 increases, the local magnetization decreases. It vanishes continuously at $J_2/J_1 \simeq 0.2075$, as shown in Fig. 5.[59] This value is in excellent agreement with recent numerical results, such as 0.2 by Mezzacapo *et al.*,[36] who use VMC with an entangled-plaquette variational ansatz, as well as 0.207 ± 0.003 by Bishop *et al.*,[37] who use CCM. The shift of the Néel boundary compared with the classical estimate $1/6$ is due to quantum fluctuations which tend to be collinear Néel rather than spiral phases in some cases.[39] In this region, the SSCF is antiferromagnetic in all directions, and the Boson condensation happens at the Γ point of the first Brillouin zone: $\mathbf{k}^* = (0,0)$, which corresponds to the ordering vector $\mathbf{Q} = (0,0)$. As J_2/J_1 decreases from 0.5, the local magnetization $M(\mathbf{Q})$ decreases. It vanishes continuously at $J_2/J_1 \simeq 0.398$, as shown in Fig. 5.[59] This value is also in good agreement with recent numerical results, such as 0.4 by Mezzacapo *et al.*,[36] as well as 0.385 ± 0.010 by Bishop *et al.*[37] In this region, the SSCF shows different properties in different directions; however, it exhibits long-range order in all directions. The gapless points of the excitation spectrum move continuously inside the first Brillouin zone as J_2/J_1 changes. These results correspond to a spiral phase. In the classical version ($S \to \infty$) of the model [see Fig. 2(a)], for $J_2/J_1 > 1/6$ there remains a line-type degeneracy in which the spiral wave number is not determined uniquely and is allowed on a ring in the Brillouin zone.[49,50] Our results suggest that the classical degeneracy is lifted in the quantum version, where some spiral wave vectors are favored by quantum fluctuations from the manifold of classically degenerate spiral wave vectors. This spiral order by disorder selection was already seen by using the spin-wave approach of Mulder *et al.*,[30] and we have recovered this selection with a different approach.

The most interesting part of the phase diagram is the intermediate region, which has no classical counterpart. In this region, the nonmagnetic ground state retains SU(2) spin rotational symmetry and the lattice translational symmetry. However, it may break the Z_3 directional symmetry of the lattice. Following Mulder *et al.*,[30] we introduce the Z_3 directional symmetry-breaking order parameter $|\psi|$, where

$$\psi = \langle \mathbf{S}_A(\mathbf{r}) \cdot \mathbf{S}_B(\mathbf{r}) \rangle + \omega \langle \mathbf{S}_A(\mathbf{r}) \cdot \mathbf{S}_B(\mathbf{r} + \mathbf{e}_1) \rangle + \omega^2 \langle \mathbf{S}_A(\mathbf{r}) \cdot \mathbf{S}_B(\mathbf{r} - \mathbf{e}_2) \rangle . \quad (32)$$

Here A and B correspond to the two different sublattices, $\mathbf{r}$ denotes the unit cell position, and $\omega = \exp(i2\pi/3)$. Equivalently, Okumura *et al.*[32] define $\mathbf{m}_3 = \varepsilon_1 \mathbf{a}_1 + \varepsilon_2 \mathbf{a}_2 + \varepsilon_3 \mathbf{a}_3$, where ε_μ ($\mu = 1,2,3$) are bond energies corresponding to the three nearest-neighbor bonds $\mathbf{a}_\mu$ ($\mu = 1,2,3$). It is trivial to see $|\psi| = |\mathbf{m}_3|$. This order parameter is zero when the spin correlations along the three directions are equal. We find that $|\psi|$ remains zero when $J_2/J_1 \lesssim 0.3732$; it becomes nonzero continuously at $J_2/J1 \simeq 0.3732$, as shown in Fig. 4.[59] Therefore, in the region $0.2075 \lesssim J_2/J_1 \lesssim 0.3732$, the ground state preserves the Z_3 lattice rotational symmetry. The SSCF shows short-range antiferromagnetic correlations in all directions, and the minimum of the excitation spectrum remains pinned at the Γ point. Namely, the system remains a GSL. The appearance of the GSL agrees with recent two different VMC studies.[33,36] In the region $0.3732 \lesssim J_2/J_1 \lesssim 0.398$, the Z_3 lattice rotational symmetry has broken. We find that the values of the mean fields A and B are $A(B)_{\mathbf{a}_2} = A(B)_{\mathbf{a}_3} \neq A(B)_{\mathbf{a}_1}$; the bond energies have the same property: $\varepsilon_2 = \varepsilon_3 \neq \varepsilon_1$. Therefore, the system should belong to the staggered-dimer VBC (lattice nematic). To further analyze this region, one needs to calculate the dimer-dimer correlations. However, it is out of the scope of the present paper. The existence of the staggered-dimer VBC is in agreement with a recent ED study,[34] a bond operator mean-field study,[30] and a VMC study.[33]

The errors in the values of the phase boundaries that are implicit here in the number of significant figures quoted correspond purely to the error in the extrapolation of our finite-size results to the thermodynamic limit. In no way are they intended to represent the essentially unknown errors implicit in the mean-field approach, e.g., the 10% difference in $M(\mathbf{Q})$ compared with the QMC result in the unfrustrated limit. All the transition values presented in this paper correspond to mean-field estimations. In order to improve these values, it is necessary to study in detail the phase transitions beyond the mean-field level, which is out of the scope of the present paper.

In Fig. 6 we show the results for the ground-state energy per unit cell extrapolated to the thermodynamic limit. For the unfrustrated case ($J_2 = 0$), $E_{gs}/N_c = -1.09779$, which is in excellent agreement with the second-order spin-wave calculation result of -1.0978.[65] Compared with published QMC results by Reger *et al.*[67] [$-1.0890(9)$] and, more recently,

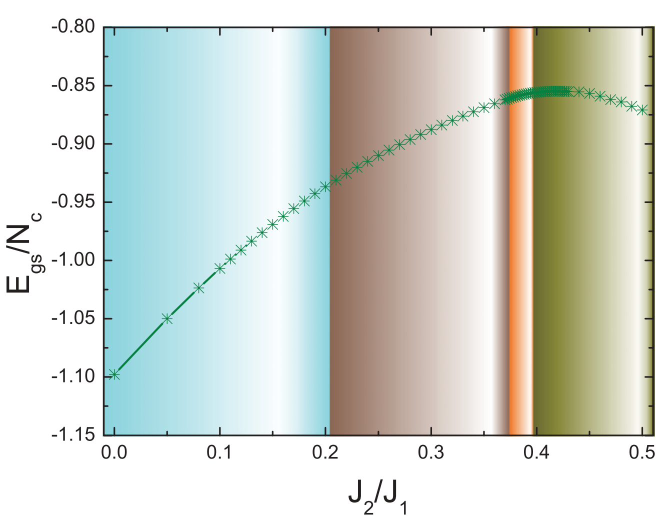

FIG. 6. (Color online) Ground-state energy per unit cell extrapolated to the thermodynamic limit as a function of the frustration J_2/J_1. The regions of the four different phases are indicated using the same colors that are used in Fig. 2.

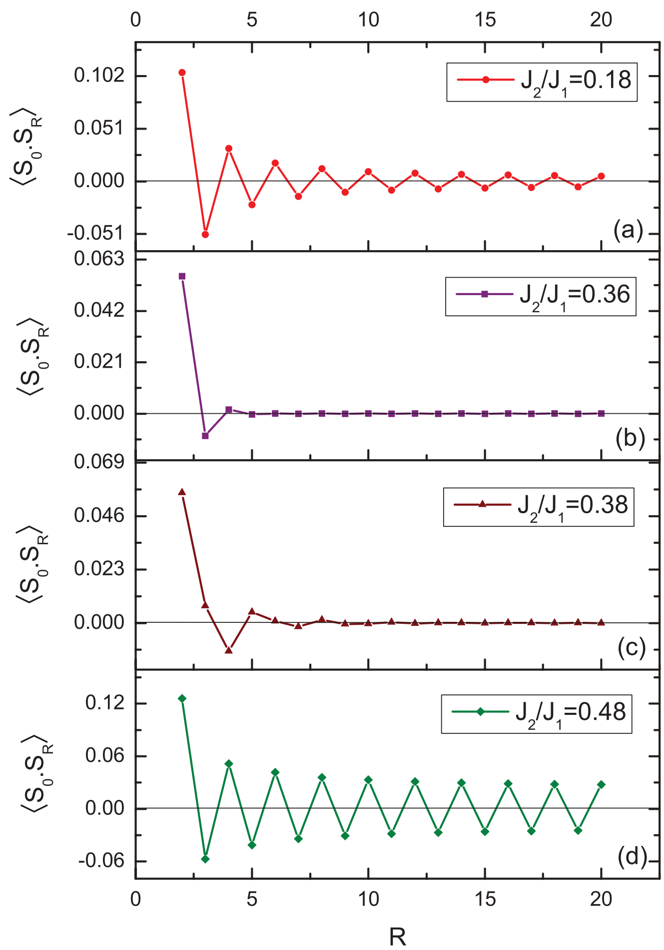

FIG. 7. (Color online) SSCF for a system of size $N = 2 \times 50 \times 50$ in the zigzag direction corresponding to the four different phases: (a) $J_2/J_1 = 0.18$ (Néel), (b) $J_2/J_1 = 0.36$ (GSL), (c) $J_2/J_1 = 0.38$ (staggered-dimer VBC), and (d) $J_2/J_1 = 0.48$ (spiral).

by Löw[68] [$-1.08909(39)$], it has appreciable difference, as mentioned in our previous discussion of the difference in the $M(\mathbf{Q})$ values. Since energy estimates always have an intrinsic quadratic error, compared to an intrinsic linear error for other properties, even small errors in the energy can be of significance. The shape of the energy curve also supports that the three quantum phase transitions are continuous.

In the following we show several typical examples for the four different phases. The SSCF along zigzag and armchair directions for a system of 5000 sites is shown in Figs. 7 and 8 for $J_2/J_1 = 0.18$ (Néel), 0.36 (GSL), 0.38 (staggered-dimer VBC), and 0.48 (spiral). The corresponding lowest excitation spectrum is shown in Fig. 9. Although it is a finite-size system, we can still see the corresponding properties for the four different phases, as we have presented above. For $J_2/J_1 = 0.18$, the SSCF in both of the zigzag and armchair directions shows long-range Néel correlations, and the lowest excitation spectrum becomes gapless at the Γ point (for a finite-size system there is a small gap which disappears after the extrapolation). For $J_2/J_1 = 0.36$, the SSCF in both the zigzag and armchair directions shows short-range Néel correlations, and the minimum of the lowest excitation spectrum remains at the Γ point; however, there is a large gap which does

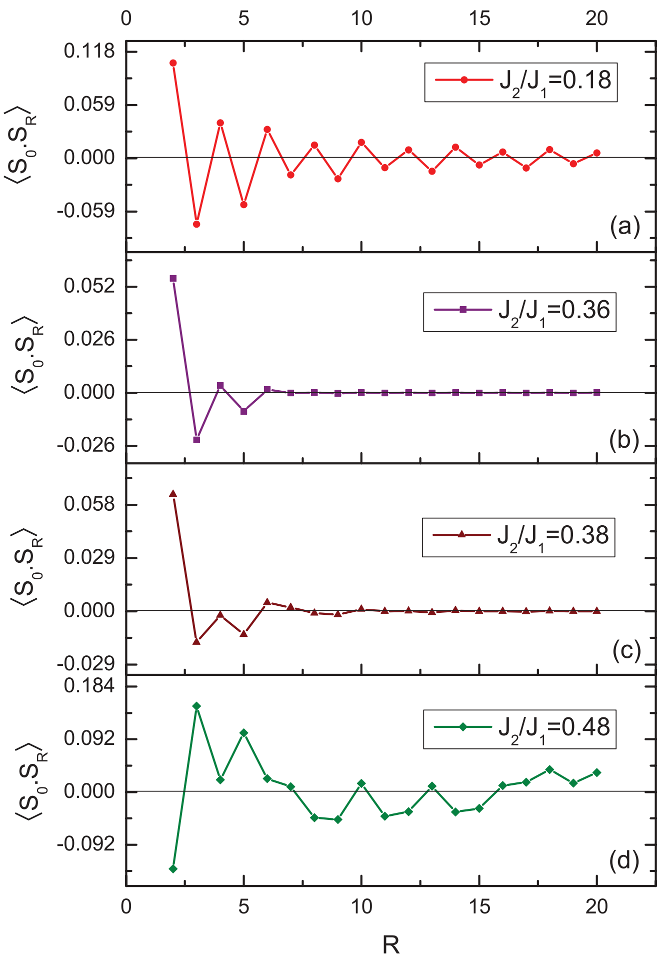

FIG. 8. (Color online) SSCF for a system of size $N = 2 \times 50 \times 50$ in the armchair direction corresponding to the four different phases: (a) $J_2/J_1 = 0.18$ (Néel), (b) $J_2/J_1 = 0.36$ (GSL), (c) $J_2/J_1 = 0.38$ (staggered-dimer VBC), and (d) $J_2/J_1 = 0.48$ (spiral).

not disappear after the extrapolation. For $J_2/J_1 = 0.38$, the SSCF does not show any long-range correlation, and the short-range correlations are different along the zigzag and armchair directions, which is an indication that the lattice rotational symmetry is broken. Simultaneously, the minimum of the lowest excitation spectrum is away from the Γ point, and the lattice rotational symmetry is clearly broken. There is also a gap in this region which remains finite in the thermodynamic limit. For $J_2/J_1 = 0.48$, the SSCF shows magnetic long-range correlations in both of the zigzag and armchair directions. Since one component of the ordering vector $Q_x = 0$ (corresponding to $k_x^* = 0$ in the lowest excitation spectrum), the SSCF is Néel-like along the zigzag directions. This result agrees well with the spin-wave calculations by Mulder *et al.*[30]

Finally, we would like to talk about the next step of our work. We have used a mean-field approach based on the Schwinger boson representation of the spin operators. This mean-field approach has the drawback of being defined in a constrained bosonic space, with unphysical configurations being allowed if this constraint is treated as an average restriction. This drawback can be, in principle, corrected by including local fluctuations of the bosonic chemical potential.[69] This correction was calculated by Trumper *et al.*[55] for the J_1-J_2 square lattice using collective coordinate methods, where a comparison between the mean-field results and the corrected results was made. However, this hard calculation allows us to calculate only some special quantities, such as the ground-state energy and the spin stiffness. The corrections developed by Trumper *et al.* could be extended to spiral phases,[70] which would allow us to investigate, for instance, the present model.

V. SUMMARY AND DISCUSSION

In the present paper, we have investigated the quantum J_1-J_2 Heisenberg model on the honeycomb lattice within a rotationally invariant version of SBMFT. In the region $J_2/J_1 \in [0,0.5]$, the quantum phase diagram of the model displays four different regions.[59] The magnetic long-range order of the Néel and spiral types is found for $J_2/J_1 \lesssim 0.2075$ and $J_2/J_1 \gtrsim 0.398$, respectively. For the spiral region, we get the spiral order from quantum disorder selection, which agrees with Mulder *et al.*,[30] who used spin-wave theory. In the intermediate region, the energy gap is finite while the local magnetization is zero, which indicates the presence of a magnetically disordered ground state. We have used the Z_3 directional symmetry-breaking order parameter $|\psi|$ defined in Eq. (32) to classify this part into two different magnetically disordered phases: one is a GSL, which shows short-range Néel correlations ($J_2/J_1 \lesssim 0.3732$), and the other is a staggered-dimer VBC (lattice nematic), which breaks the Z_3 directional symmetry ($J_2/J_1 \gtrsim 0.3732$). Considering the properties of order parameters and the ground state energy, these three quantum phase transitions seem to be continuous.

As we have mentioned above, recent theoretical studies of the phase diagram of the spin-1/2 J_1-J_2 Heisenberg model on the honeycomb lattice have obtained conflicting results. The central controversial point is the existence and nature of magnetically disordered phases when the Néel order becomes unstable while increasing the frustration J_2/J_1. There is a growing consensus[30,33,34,36,37,39,42,45,50] that a magnetically disordered region should appear. However, the nature of this region is still not clear, with different approaches giving different results. An early ED work by Fouet *et al.*[50] first claimed that a GSL might appear in the region $J_2/J_1 \approx 0.3$–0.35, and for $J_2/J_1 \approx 0.4$ the system might be in favor of the staggered-dimer VBC. A recent ED study by Mosadeq *et al.*[34] has claimed that a plaquette valence bond crystal (PVBC) might exist in the region $0.2 < J_2/J_1 < 0.3$, and a phase transition from PVBC to the staggered-dimer VBC exists at a point of the region $0.35 \leqslant J_2/J_1 \leqslant 0.4$. However, a more recent ED work by Albuquerque *et al.*,[39] which has treated larger system sizes, has been unable to discriminate whether this magnetically disordered region corresponds to PVBC with a small-order parameter or a GSL. It is possible that the PVBC may just come from the finite-size effects.[36] For larger J_2/J_1, it has been also hard to discriminate the staggered dimer VBC with spiral phases, since it is especially difficult to use ED to treat the incommensurate behavior of spin correlations due to the small lattice sizes.

There are two recent studies of this model using VMC with different variational wave functions. Clark *et al.*[33] have used Huse-Elser states and resonating valence bond (RVB) states and claimed that a GSL appears in the region

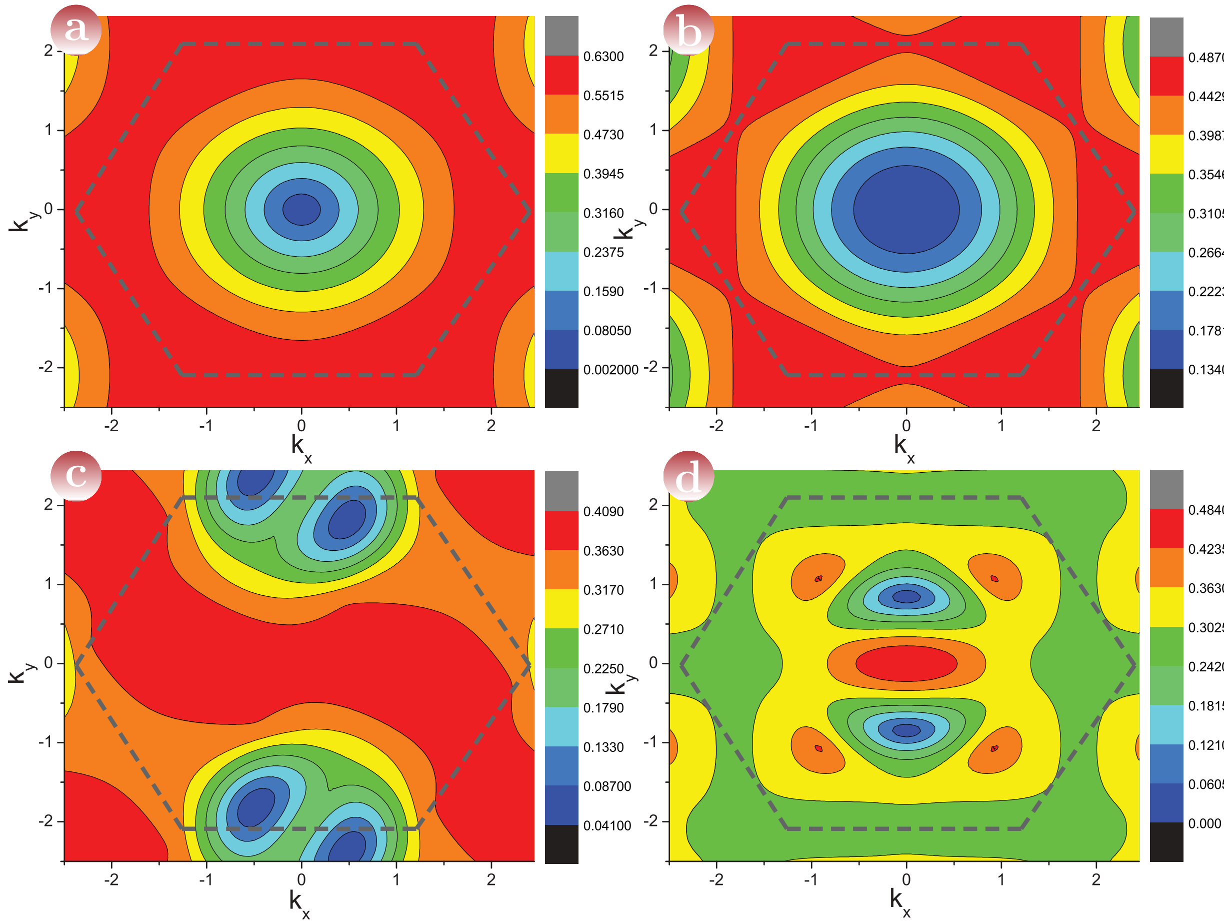

FIG. 9. (Color online) Momentum dependence of the lowest excitation spectrum for a system of size $N = 2 \times 50 \times 50$ corresponding to the four different phases: (a) $J_2/J_1 = 0.18$ (Néel), (b) $J_2/J_1 = 0.36$ (GSL), (c) $J_2/J_1 = 0.38$ (staggered-dimer VBC), and (d) $J_2/J_1 = 0.48$ (spiral). The dashed hexagon denotes the first Brillouin zone of the lattice.

$0.08 \leqslant J_2/J_1 \leqslant 0.3$, a dimerized state which breaks lattice rotational symmetry for $J_2/J_1 \gtrsim 0.3$. However, a more recent work by Mezzacapo *et al.*[36] using an entangled-plaquette variational (EPV) ansatz has obtained lower energy estimates and claimed that in the magnetically disordered region $0.2 \lesssim J_2/J_1 \lesssim 0.4$, the PVBC order parameter vanishes in the thermodynamic limit. Therefore, the PVBC may just come from the finite-size effects. Since the Z_3 directional symmetry-breaking order parameter has not been considered in this paper, it is still not clear whether the lattice rotational symmetry is broken or not in the region $0.2 \lesssim J_2/J_1 \lesssim 0.4$.

In a recent study using PFFRG[42] the authors have obtained that within the magnetically disordered region, for larger J_2/J_1, there is a strong tendency for the staggered-dimer ordering; for low J_2/J_1, both plaquette and staggered-dimer responses are very weak. A further recent study using CCM[37] has got a more quantitative magnetically disordered region: $0.207 \pm 0.003 < J_2/J_1 < 0.385 \pm 0.010$, in which the PVBC phase has been reported. However, the ground state within $0.21 \lesssim J_2/J_1 \lesssim 0.24$ is hard to determine using this approach.

The other controversial point is the form of the magnetic long-range order when J_2/J_1 exceeds the magnetically disordered region. There are two proposals: the anti-Néel order[37] and the spiral order. It is difficult to get a conclusion by ED since it is hard to use it to treat the incommensurate spin correlations due to small lattice sizes.[39] Neither of the recent SE[40] and PFFRG[42] studies have found any evidence for the existence of the anti-Néel order, and they concluded that the spiral state should be the stable ground state. However, both the VMC with EPV ansatz[36] and the CCM[37] studies support the opposite proposal. Since we are interested in the exotic disordered phases in the magnetically disordered region and focus on $J_2/J_1 \in [0,0.5]$, we cannot exclude the possibility that the anti-Néel order state exists for $J_2/J_1 > 0.5$.

Due to the existence of strong quantum fluctuations and frustration, the spin-$1/2$ J_1-J_2 Heisenberg model on the honeycomb lattice is a challenging model which needs further investigation, especially for the nature of the intermediate phase. Unbiased numerical simulations are still needed, such as the density matrix renormalization group (DMRG) method.[71–73] Recently, DMRG has been applied to the spin-$1/2$ kagome Heisenberg model[74,75] and the spin-$1/2$ square J_1-J_2 Heisenberg model[76] and obtained GSLs as the ground state. Since quantum fluctuations are expected to be stronger on the honeycomb lattice than those on the square lattice, it would be very interesting to apply DMRG to the spin-$1/2$ J_1-J_2 Heisenberg model on the honeycomb lattice.

ACKNOWLEDGMENTS

We are especially grateful to Hirokazu Tsunetsugu for his suggestion of this project and numerous enlightening discussions for numerical calculations. We would like to thank Peng Li for fruitful discussions. H.Z. is supported by the Japanese Government Scholarship from MEXT of Japan. C.A.L. is partially supported by CONICET (PIP 1691) and ANPCyT (PICT 1426).

*Corresponding author: zhanghao@issp.u-tokyo.ac.jp

[1] H. A. Bethe, Z. Phys. **71**, 205 (1931).
[2] W. Zheng and C. J. Hamer, Phys. Rev. B **47**, 7961 (1993).
[3] A. W. Sandvik, Phys. Rev. B **56**, 11678 (1997).
[4] P. W. Anderson, Mater. Res. Soc. Bull. **8**, 153 (1973); P. Fazekas and P. W. Anderson, Philos. Mag. **30**, 423 (1974); P. W. Anderson, Science **235**, 1196 (1987).
[5] M. A. Metlitski and S. Sachdev, Phys. Rev. B **77**, 054411 (2008).
[6] R. K. Kaul, M. A. Metlitski, S. Sachdev, and C. Xu, Phys. Rev. B **78**, 045110 (2008).
[7] L. Wang and A. W. Sandvik, Phys. Rev. B **81**, 054417 (2010).
[8] R. Moessner, S. L. Sondhi, and P. Chandra, Phys. Rev. B **64**, 144416 (2001).
[9] A. Ralko, M. Mambrini, and D. Poilblanc, Phys. Rev. B **80**, 184427 (2009).
[10] A. Mattsson, P. Fröjdh, and T. Einarsson, Phys. Rev. B **49**, 3997 (1994).
[11] K. Takano, Phys. Rev. B **74**, 140402 (2006).
[12] M. Hermele, Phys. Rev. B **76**, 035125 (2007).
[13] R. Kumar, D. Kumar, and B. Kumar, Phys. Rev. B **80**, 214428 (2009).
[14] O. Smirnova, M. Azuma, N. Kumada, Y. Kusano, M. Matsuda, Y. Shimakawa, T. Takei, Y. Yonesaki, and N. Kinomura, J. Am. Chem. Soc. **131**, 8313 (2009).
[15] S. Okubo, F. Elmasry, W. Zhang, M. Fujisawa, T. Sakurai, H. Ohta, M. Azuma, O. A. Sumirnova, and N. Kumada, J. Phys. Conf. Series **200**, 022042 (2010).
[16] M. Matsuda, M. Azuma, M. Tokunaga, Y. Shimakawa, and N. Kumada, Phys. Rev. Lett. **105**, 187201 (2010).
[17] M. Azuma, M. Matsuda, N. Onishi, S. Olga, Y. Kusano, M. Tokunaga, Y. Shimakawa, and N. Kumada, J. Phys. Conf. Series **320**, 012005 (2011).
[18] *Magnetic Properties of Layered Transition Metal Compounds*, edited by L. J. De Jongh (Kluwer, Dordrecht, 1990).
[19] A. Möller, U. Löw, T. Taetz, M. Kriener, G. André, F. Damay, O. Heyer, M. Braden, and J. A. Mydosh, Phys. Rev. B **78**, 024420 (2008).
[20] A. A. Tsirlin, O. Janson, and H. Rosner, Phys. Rev. B **82**, 144416 (2010).
[21] A. H. Castro Neto, F. Guinea, N. M. R. Peres, K. S. Novoselov, and A. K. Geim, Rev. Mod. Phys. **81**, 109 (2009).
[22] Z. Y. Meng, T. C. Lang, S. Wessel, F. F. Assaad, and A. Muramatsu, Nature (London) **464**, 847 (2010).
[23] F. Wang, Phys. Rev. B **82**, 024419 (2010).
[24] Y.-M. Lu and Y. Ran, Phys. Rev. B **84**, 024420 (2011).
[25] H. Y. Yang and K. P. Schmidt, Europhys. Lett. **94**, 17004 (2011).
[26] A. Vaezi and X. G. Wen, arXiv:1010.5744.
[27] A. Vaezi, M. Mashkoori, and M. Hosseini, Phys. Rev. B **85**, 195126 (2012).
[28] M.-T. Tran and K.-S. Kim, Phys. Rev. B **83**, 125416 (2011).
[29] S. Sorella, Y. Otsuka, and S. Yunoki, Sci. Rep. **2**, 992 (2012).
[30] A. Mulder, R. Ganesh, L. Capriotti, and A. Paramekanti, Phys. Rev. B **81**, 214419 (2010).
[31] R. Ganesh, D. N. Sheng, Y.-J. Kim, and A. Paramekanti, Phys. Rev. B **83**, 144414 (2011).
[32] S. Okumura, H. Kawamura, T. Okubo, and Y. Motome, J. Phys. Soc. Jpn. **79**, 114705 (2010).
[33] B. K. Clark, D. A. Abanin, and S. L. Sondhi, Phys. Rev. Lett. **107**, 087204 (2011).
[34] H. Mosadeq, F. Shahbazi, and S. A. Jafari, J. Phys. Condens. Matter **23**, 226006 (2011).
[35] H. D. Rosales, D. C. Cabra, C. A. Lamas, P. Pujol, and M. E. Zhitomirsky, arXiv:1208.2416.
[36] F. Mezzacapo and M. Boninsegni, Phys. Rev. B **85**, 060402(R) (2012).
[37] R. F. Bishop, P. H. Y. Li, D. J. J. Farnell, and C. E. Campbell, J. Phys. Condens. Matter **24**, 236002 (2012).
[38] D. C. Cabra, C. A. Lamas, and H. D. Rosales, Phys. Rev. B **83**, 094506 (2011).
[39] A. F. Albuquerque, D. Schwandt, B. Hetényi, S. Capponi, M. Mambrini, and A. M. Läuchli, Phys. Rev. B **84**, 024406 (2011).
[40] J. Oitmaa and R. R. P. Singh, Phys. Rev. B **84**, 094424 (2011).
[41] D. J. J. Farnell, R. F. Bishop, P. H. Y. Li, J. Richter, and C. E. Campbell, Phys. Rev. B **84**, 012403 (2011).
[42] J. Reuther, D. A. Abanin, and R. Thomale, Phys. Rev. B **84**, 014417 (2011).
[43] P. H. Y. Li, R. F. Bishop, D. J. J. Farnell, J. Richter, and C. E. Campbell, Phys. Rev. B **85**, 085115 (2012).
[44] R. F. Bishop and P. H. Y. Li, Phys. Rev. B **85**, 155135 (2012).
[45] P. H. Y. Li, R. F. Bishop, D. J. J. Farnell, and C. E. Campbell, Phys. Rev. B **86**, 144404 (2012).
[46] X. G. Wen, Phys. Rev. B **44**, 2664 (1991).
[47] C. Lhuillier and G. Misguich, in *Introduction to Frustrated Magnetism*, edited by C. Lacroix, P. Mendels, and F. Mila (Springer, Berlin, 2011).
[48] S. Katsura, T. Ide, and T. Morita, J. Stat. Phys. **42**, 381 (1986).
[49] E. Rastelli, A. Tassi, and L. Reatto, Phys. B **97**, 1 (1979).
[50] J. B. Fouet, P. Sindzingre, and C. Lhuillier, Eur. Phys. J. B **20**, 241 (2001).
[51] T. Einarsson and H. Johannesson, Phys. Rev. B **43**, 5867 (1991).
[52] R. Flint and P. Coleman, Phys. Rev. B **79**, 014424 (2009).
[53] H. A. Ceccatto, C. J. Gazza, and A. E. Trumper, Phys. Rev. B **47**, 12329 (1993).
[54] C. J. Gazza and H. A. Ceccatto, J. Phys. Condens. Matter **5**, L135 (1993).
[55] A. E. Trumper, L. O. Manuel, C. J. Gazza, and H. A. Ceccatto, Phys. Rev. Lett. **78**, 2216 (1997).
[56] A. Mezio, C. N. Sposetti, L. O. Manuel, and A. E. Trumper, Europhys. Lett. **94**, 47001 (2011).
[57] H. Feldner, D. C. Cabra, and G. L. Rossini, Phys. Rev. B **84**, 214406 (2011).

[58] L. Messio, B. Bernu, and C. Lhuillier, Phys. Rev. Lett. **108**, 207204 (2012).
[59] The errors in the values of the phase boundaries which are implicit in the number of significant figures quoted only reflect the error in the extrapolation of our finite-size results to the thermodynamic limit. They are not intended to represent the essentially unknown errors implicit in the mean-field approach, e.g., the differences in the local magnetization and the ground-state energy per unit cell compared with the QMC results in the unfrustrated limit.
[60] D. P. Arovas and A. Auerbach, Phys. Rev. B **38**, 316 (1988); A. Auerbach and D. P. Arovas, Phys. Rev. Lett. **61**, 617 (1988).
[61] A. Auerbach, *Interacting Electrons and Quantum Magnetism* (Springer, New York, 1994).
[62] A. Auerbach and D. P. Arovas, in *Introduction to Frustrated Magnetism*, edited by C. Lacroix, P. Mendels, and F. Mila (Springer, Berlin, 2011).
[63] J. E. Hirsch and S. Tang, Phys. Rev. B **39**, 2850 (1989).
[64] J. H. P. Colpa, Phys. A **93**, 327 (1978).
[65] W. Zheng, J. Oitmaa, and C. J. Hamer, Phys. Rev. B **44**, 11869 (1991).
[66] E. V. Castro, N. M. R. Peres, K. S. D. Beach, and A. W. Sandvik, Phys. Rev. B **73**, 054422 (2006).
[67] J. D. Reger, J. A. Riera, and A. P. Young, J. Phys. Condens. Matter **1**, 1855 (1989).
[68] U. Löw, Condens. Matter Phys. **12**, 497 (2009).
[69] M. Raykin and A. Auerbach, Phys. Rev. Lett. **70**, 3808 (1993).
[70] L. O. Manuel, A. E. Trumper, and H. A. Ceccatto, Phys. Rev. B **57**, 8348 (1998).
[71] S. R. White, Phys. Rev. Lett. **69**, 2863 (1992).
[72] S. R. White and A. L. Chernyshev, Phys. Rev. Lett. **99**, 127004 (2007).
[73] E. M. Stoudenmire and S. R. White, Annu. Rev. Condens. Matter Phys. **3**, 111 (2012).
[74] S. M. Yan, D. A. Huse, and S. R. White, Science **332**, 1173 (2011).
[75] S. Depenbrock, I. P. McCulloch, and U. Schollwöck, Phys. Rev. Lett. **109**, 067201 (2012).
[76] H. C. Jiang, H. Yao, and L. Balents, Phys. Rev. B **86**, 024424 (2012).